Journal of New Technology and Materials(JNTM)
J. New Technol. Mater.
Vol. 07, N°02 (2017)10-21

OEB Univ. Publish.Co.

Effect of fin spacing on turbulent heat transfer in a channel with cascaded rectangular-triangular fins

Younes Menni* and Ahmed Azzi

Unit of Research on Materials and Renewable Energies - URMER -

Department of Physics, Faculty of Sciences, Abou Bekr Belkaid University, BP 119 - 13000 - Tlemcen – Algeria

*Corresponding author, email: menniyounes.cfd@gmail.com

Received date: Feb 13, 2017; revised date: Dec 10, 2017; accepted date: Dec 16, 2017

Abstract

Through this work, we performed a two-dimensional analysis of a constant property fluid (air) flowing into a rectangular cross section channel with staggered cascaded rectangular-triangular shaped fins (CRTFs). The governing flow equations, i.e., continuity, momentum, turbulence, and energy equations, employed to simulate the incompressible steady fluid and heat transfer in the whole domain investigated, were solved by the finite volumes approach, in two dimensions, employing the Computational Fluid Dynamics, Commercial Software FLUENT with the low-Reynolds-numberk-ε model to describe the turbulence phenomenon. The simulations were conducted for the channel of aspect ratio, AR = 1.32 and aeraulic diameter, D_h = 0.167 m with five different finspacing, (S = Pi/2, 3Pi/4, Pi, 5Pi/4 and 3Pi/2) and five various Reynolds number values, (Re = 10,000, 15,000, 20,000, 25,000, and 30,000) while the CRTF height-to-channel height blockage ratio, BR is set to 0.55 and kept constant. The velocity and pressure fields, skin friction loss, and local and average Nusselt numbers were obtained at constant surface temperature condition along the upper and lower surfaces of the channel.The analysis of the numerical results proved that both the Reynolds number and the CRTF separation distance had an effect on the dynamic and thermal behavior of air in the given computational domain. The Nusselt numbers and skin friction coefficients increase with the rise in the Reynolds number but decrease with the increase in the fin spacing. By comparing with those implemented in practice, our numerical results are very agreeable. This analysis can be applied in improving the thermal efficiency of solar air collectors as well as heat exchangers.

Keywords: Cascaded rectangular-triangular fin; CFD; Channel; Flow dynamics; Forced convection; Pressure drop

1. Introduction

Different strategies, based on both active and passive techniques, were conducted to improve the convective heat transfer in many engineering applications such asshell-and-tube heat exchangers, solar air collectors and electronic packages. Among these methods are channelscontaining deflectors such as baffles and fins.

Measurements using laser-Doppler anemometry technique in the turbulent flow through a channel with several baffle plates were performed by Berner et al. [1] with the purpose of determining the number of baffles necessary for obtaining a periodic boundary condition and the dependence on Reynolds number and the geometry.

Kellar and Patankar [2] simulated the laminar flow with heat transfer between parallel plates with staggered fins and found that the flow is characterized by strong deformations, large recirculation regions, and in general, the Nusselt number and skin friction increase with the Reynolds number.

A computational work of laminar heat transfer in a three-dimensional channel fitted with baffles at uniform wall heat flux condition along the upper and lower channel wall was presented by Lopez et al. [3].

Tsay et al. [4] investigated numerically by using baffles for internal cooling augmentation in laminar channel flow over two heated blocks mounted on the lower plate.

By means of hot wire experiments and numerical simulation, Demartini et al. [5] presented the analysis of the pressure and velocity field of air inside a channel of rectangular section, where two baffle plates were placed in opposite walls. The geometry of the problem is a simplification of the geometry of baffle plates found in shell-and-tube heat exchangers. The most important features observed are the high pressure regions formed upstream of both baffle plates, and the extent of the low pressure regions on the downstream regions.

Habib et al. [6] carried out an experiment for turbulent flow with heat transfer inside the periodic cell formed between segmented baffles staggered in a rectangular duct and found that the heat transfer and flow resistance

parameters increase with increasing Reynolds number and baffle height.

Mousavi and Hooman [7] reported the heat transfer aspect in the entrance region of a channel with staggered baffles for Reynolds numbers ranging from50 to 500 and baffle heights between 0 and 0.75 and observed that the Prandtl number affects the precise location of the periodically fully developed region.

The heat transfer enhancement in a heat exchanger tube by installing a baffle was conducted by Nasiruddin and Kamran Siddiqui [8]. In that study, the effect of baffle size and orientation on the heat transfer enhancement was studied in detail.

The flow field in a rectangular enclosure with length to width ratio of 1 and varying number of baffle plates were experimentally investigated by Gowda et al. [9]. The length of the baffle plates is systematically varied for a given number of baffles. They reported that both the number of baffle plates and their relative length have a significant effect on the flow field giving rise to the possibility of varying turbulent intensity and the retention time in different situations.

An optimization program was established by Saffar-Avval and Damangir [10] to calculate the optimum baffle spacing and the number of sealing strips for all types of shell and tube heat exchangers, using the procedure in the Heat Exchanger Design Handbook. After a sufficient development distance, they achieved a stream-wise periodic flow. They found this development distance to be a function of both the Reynolds number and the geometry of the baffle.

Li and Kottke [11] treated the local heat transfer and pressure drop in simulating models of shell-and-tube heat exchangers with segmental baffles. The effects of the distance between the baffles as well as Reynolds numbers were examined. They found that for a constant value of the Reynolds number, the heat exchange coefficient and pressure drop are increased by increased baffle spacing due to a reduced leakage through the baffle-shell clearance.

Tsay et al. [12] numerically analyzed the heat transfer enhancement of backward-facing step flow in a channel by using baffle installation on the channel wall. The effects of the dimensionless baffle height, baffle thickness, and distance between the backward-facing step and baffle on the flow structure, temperature distribution and Nusselt number variation were simulated in detail for a range of Reynolds number varying from 100 to 500.

Mohammadi Pirouz et al. [13] studied numerically the conjugate heat transfer for laminar and incompressible flow of fluid circulating through the channel with lower and upper wall-mounted obstacles using the Lattice Boltzmann Method. The parameters of the numerical work were the Reynolds number, thermal diffusivity and the distance between obstacles.

Dutta and Dutta [14], Dutta and Hossain [15], and Dutta et al. [16] reported the enhancement of heat transfer with inclined solid and perforated baffles. In those studies, the effects of baffle size, position, and orientation were studied for internal cooling heat transfer augmentation.

Other investigators examined in detail the impact of the shape geometry of the baffles and fins on the heat transfer phenomenon in the heat exchanger and solar air channels, i.e., rectangular [17], rounded [18], graded [19], corrugated [20], arc [21], waisted triangular [22], L [23], diamond [24], and bar [25].All these structure rise the thermal transfer rate but with large friction loss.

The purpose of this article is to investigate and examine numerically the turbulent forced-convection heat transfer and flow resistance characteristics for a 2D incompressible flow of a Newtonian fluid (air) in a rectangular channel of rectangular section with staggered cascaded rectangular-triangular fins (CRTFs) at constant surface temperature conditions. The parameters of this computational fluid dynamic analysis are the Reynolds number and the distance between the CRTFs.

2. Position of the Problem

2.1. Computational domain

The flow system is a two-dimensional horizontal rectangular cross section channel with two transverse fins placed on opposite heated walls as shown in Fig.1(a). The important geometry parameters of the system are listed in Table I.

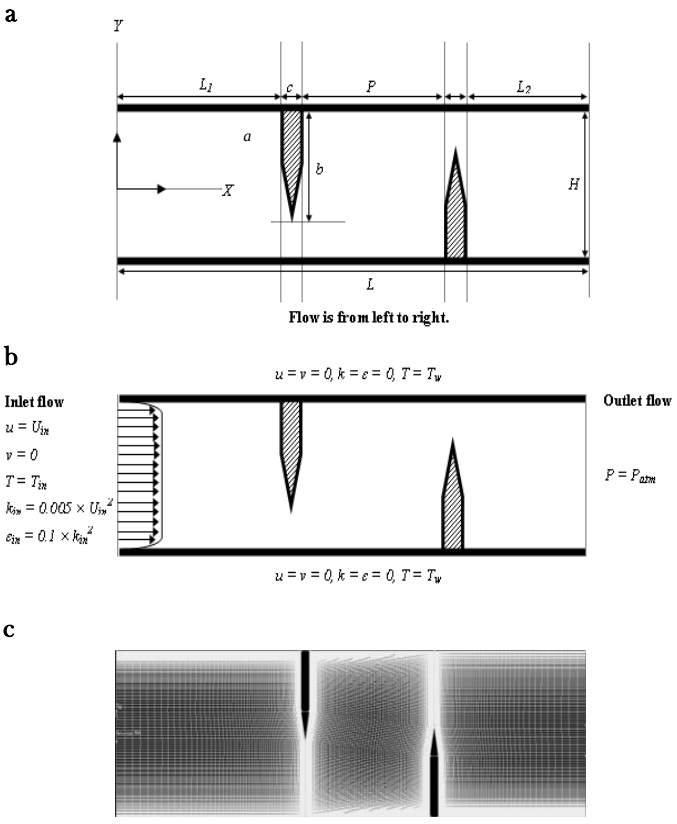

Fig. 1. Structure under investigation (a) baffled channel geometry,(b) boundary conditions, and (c) grids

The structural parameters of the present duct, cited above, is the same as the baffled channel of Demartini et al. [5] used for validation. In that study, the flow of turbulent air through a horizontal channel containing two upper and lower wall-attached baffle plates was examined.

The obstacle model under CFD simulation is a cascaded rectangular-triangular shaped, solid-type fin (CRTF). It is triangular shaped-surface of height, a, in cascade with a rectangular-shaped surface such that the overall size of assembly is b, and a/b is fixed at 0.25. The base thickness of the CRTF assembly is assumed to be c, equal to 0.01m. The computations are reported for the aspect ratio, AR = 1.32 and aeraulic diameter, D_h=0.167 m with fivevarious CRTF separation distances, (S = Pi/2, 3Pi/4, Pi, 5Pi/4 and 3Pi/2) while the blockage ration, RB is set to 0.55 and kept constant. Also, a flat rectangular solid-type fin pair (or simple baffle plates, a/b = 0) with the same geometrical dimensions b and c (but their volume is variable) is introduced for verification and validation of our numerical results.

Parameters of test channel [Unit: m]	Values
Channel length, L	0.554
Channel height, H	0.146
Channel width, W	0.193
Aeraulic diameter, D_h	0.167
Fin thickness, c	0.01
Fin height, b	0.08
Fin distance or spacing, Pi	0.142
Distance upstream of the first fin, L_1	0.218
Distance downstream of the second fin, L_2	0.174

Table I. Geometric parameters of the CRTF channel

Air is the working fluid with the Reynolds number ranging from10^4 to 3×10^4. The thermo-physical data of the air at 300 K is given in Table II. For a rectangular duct with two-CRTFs, a uniform air velocity was introduced at the inlet while anatmospheric pressure outlet condition was applied at the exit, as shown in Fig.1(b) [5]. The pressure at the channel inlet was set equal to the zero (gauge) [8]. The turbulence intensity was kept at 2 % at the inlet [5]. Impermeable and no-slip wall conditions have been implemented over the channel walls as well as the CRTF surface. The temperatures of all solid boundaries and inlet fluid are set as constant, which are 375 K and 300 K, respectively [8].

Parameter	Value	Unit
Temperature, T	300	K
Density, ρ	1.225	Kg m^{-3}
Specific heat at constant pressure, Cp	1006.43	J $Kg^{-1}K^{-1}$
Thermal conductivity, λ	0.0242	W m^{-1} s^{-1}
Dynamic viscosity, μ	1.7894×10^{-5}	Kg m^{-1} s^{-1}

Table II. Thermo-physical data of air at 300 K

The channel model with CRTFs is discretized with structured quadrilateral-type elements, and the regions near the solid surfaces are meshed better [5,8] to resolve the strong gradients of velocity, temperature and pressure in that region, as shown in Fig.1(c). For the regions more distant from the walls, the mesh is uniform, as indicated by Demartini et al.[5]. To examine the effect of the mesh size on the CFD solution, various meshvalues are verified and a mesh system of cells of370 × 145, in X and Y directionsrespectively, is chosen.

2.2. Boundary conditions

The aerodynamic boundary conditions are set according to the numerical and experimental analysis of Demartini et al. [5] while the thermal boundary conditions are chosen according to the simulation of Nasiruddin and Kamran Siddiqui [8]. The baffled channel and boundary condition, as shown in Fig. 1(b), are presented as

(1) At the inlet (x = 0, -H/2 ≤ y ≤ H/2):

$$u = U_{in} \quad \text{and} \quad v = 0 \tag{1}$$

$$T = T_{in} \tag{2}$$

$$k_{in} = 0{,}005.U_{in}^2 \tag{3}$$

$$\varepsilon_{in} = 0{,}1.k_{in}^{3/2} \tag{4}$$

(2) At the walls (top wall: 0 ≤ x ≤ L, y = H/2, and bottom wall: 0 ≤ x ≤ L, y = -H/2):

$$u = v = 0 \tag{5}$$

$$T = T_w \tag{6}$$

$$k = \varepsilon = 0 \tag{7}$$

(3) At the solid/fluid interface, the following condition is applied:

$$\lambda_f \left.\frac{\partial T_f}{\partial x}\right|_{\vec{N}} = \lambda_s \left.\frac{\partial T_s}{\partial x}\right|_{\vec{N}} \tag{8}$$

$$T_f\big|_{\vec{N}} = T_s\big|_{\vec{N}} \tag{9}$$

(4) At the exit (x = L, -H/2 ≤ y ≤ H/2):

$$P = P_{atm} \tag{10}$$

$$\frac{\partial u}{\partial x} = \frac{\partial v}{\partial x} = \frac{\partial T}{\partial x} = \frac{\partial k}{\partial x} = \frac{\partial \varepsilon}{\partial x} = 0 \tag{11}$$

where $\vec{N}$ is the vector normal to the considered surface interface, λ and λ are the thermal conductivities of fluid and solid, respectively.

2.3. Numerical models

The numerical model for turbulent forced-convection heat transfer in a rectangular channel with two-CRTFs was simulated under the following assumptions:

- Steady two-dimensional fluid flow and heat transfer.
- The flow is turbulent and incompressible.
- Constant fluid properties.
- Body forces and viscous dissipation are ignored.
- Negligible radiation heat transfer.

3. Mathematical modeling

3.1. Governing equations

The computational domain fitted with two cascaded rectangular-triangular fins is simulated by using Computational Fluid Dynamics (CFD), Commercial software FLUENT. The k-εturbulence model at low-Reynolds-number proposed by Jones and Launder [26] is adopted in this study. In Cartesian coordinate, the continuity, momentum, energy and turbulence equations for a steady two-dimensional incompressible flow of a Newtonian fluid can be written in the following compact form Patankar [27]:

$$\frac{\partial}{\partial x}(\rho u\phi)+\frac{\partial}{\partial y}(\rho v\phi)=\frac{\partial}{\partial x}\left[\Gamma_\phi\frac{\partial\phi}{\partial x}\right]+\frac{\partial}{\partial y}\left[\Gamma_\phi\frac{\partial\phi}{\partial y}\right]+S_\phi \qquad (12)$$

whereϕ is a vector composed of the scalars u, v, T, k and ε. u and v stand for the local mean velocities towards the axis x and y, respectively. T is the temperature. k and ε stand for turbulent kinetic energy and turbulent dissipation rate, respectively. Γ_ϕ and S_ϕ represent the turbulent diffusion coefficient and the source term associated with the general variableϕ in this order. The expressions ofϕ, $\Gamma_\phi$and S_ϕ are presented for:

Continuity equation

$$\phi = 1 \qquad (13)$$

$$\Gamma_\phi = 0 \qquad (14)$$

$$S_\phi = 0 \qquad (15)$$

Momentum equation in X-direction

$$\phi = u \qquad (16)$$

$$\Gamma_\phi = \mu_e \qquad (17)$$

$$S_\phi = -\frac{\partial p}{\partial x}+\frac{\partial}{\partial x}\left[\mu_e\left(\frac{\partial u}{\partial x}\right)\right]+\frac{\partial}{\partial y}\left[\mu_e\left(\frac{\partial v}{\partial x}\right)\right] \qquad (18)$$

Momentum equation in Y-direction

$$\phi = v \qquad (19)$$

$$\Gamma_\phi = \mu_e \qquad (20)$$

$$S_\phi = -\frac{\partial p}{\partial y}+\frac{\partial}{\partial x}\left[\mu_e\left(\frac{\partial u}{\partial y}\right)\right]+\frac{\partial}{\partial y}\left[\mu_e\left(\frac{\partial v}{\partial y}\right)\right] \qquad (21)$$

Energy equation

$$\phi = T \qquad (22)$$

$$\Gamma_\phi = \frac{\mu_e}{\sigma_T} \qquad (23)$$

$$S_\phi = 0 \qquad (24)$$

k-turbulent kinetic energy equation

$$\phi = \mathrm{k} \qquad (25)$$

$$\Gamma_\phi = \mu_\ell + \frac{\mu_t}{\sigma_k} \qquad (26)$$

$$S_\phi = -\rho.\varepsilon + G \qquad (27)$$

ε-turbulent dissipation rate equation

$$\phi = \varepsilon \qquad (28)$$

$$\Gamma_\phi = \mu_\ell + \frac{\mu_t}{\sigma_\varepsilon} \qquad (29)$$

$$S_\phi = \left(C_{1\varepsilon} f_1 G - C_{2\varepsilon} f_2 \rho.\varepsilon\right)\frac{\varepsilon}{k} \qquad (30)$$

with

$$G = \mu_t\left\{2.\left(\frac{\partial u}{\partial x}\right)^2+2.\left(\frac{\partial v}{\partial y}\right)^2+\left(\frac{\partial v}{\partial x}+\frac{\partial u}{\partial y}\right)^2\right\} \qquad (31)$$

$$\mu_e = \mu_\ell + \mu_t \qquad (32)$$

$$\mu_t = f_\mu \rho.C_\mu \frac{k^2}{\varepsilon} \qquad (33)$$

where C_μ = 0.09; $C_{1\varepsilon}$ = 1.44; $C_{2\varepsilon}$ = 1.92; σ_k = 1.0; σ_ε= 1.3; σ_T = 0.9 are the constants of the model, as proposed by Laundry and Spalding [28].

3.2. Numerical methods and computational details

The CFD software FLUENTwas used to simulate the fluid flow and heat transfer distributions. The governing equations were discretized using the Finite Volume Method (FVM), details of which can be found in Patankar [27]. The SIMPLEC discretization algorithm (Semi-Implicit Method for Pressure-Linked Equations) [29] was adopted. The diffusion terms appearing in the transport equations for momentum and turbulence parameters are discretized using Second-Order Central Differencing (SOCD) [29]. The Power-Law Differencing Scheme (PLDS) of Patankar [29] was used to approximate the convection terms. The discretized governing equation is typically solved using the Tri-Diagonal Matrix Algorithm (TDMA) [29]. The solutions were considered to be converged when the normalized residual values were less than 10^{-6} for all variables $\phi \equiv$ (u, v, k, ε) but less than 10^{-9} only for the energy equation $\phi \equiv$ (T).

The Reynolds number, of the experiments [5] is Re = 8.73×10^4, calculated with the aeraulic diameter of the channel, D_h, and the entrance velocity ($\overline{U}$) as [5]

$$\mathrm{Re} = \frac{\rho \overline{U} D_h}{\mu} \qquad (34)$$

The skin friction coefficient (Cf) is defined by[30]

$$Cf = \frac{2\tau_w}{\rho \overline{U}^2} \qquad (35)$$

The friction factor (f) is computed by pressure drop (ΔP) across the length of the rectangular channel (L) as[30]

$$f = \frac{(\Delta P / L) D_h}{\frac{1}{2}\rho \overline{U}^2} \qquad (36)$$

whereρ is the fluid density, μ the dynamic viscosity of fluid, and τ_w the rate of shearing to the wall.

The friction factor for a smooth channel (f_0) is calculated from the correlation developed by Petukhov [31] as follows:

$$f_0 = \left(0.79 \ln \mathrm{Re} - 1.64\right)^{-2} \quad \text{and} \quad 3{,}000 \le \mathrm{Re} \le 5 \times 10^6 \qquad (37)$$

The heat transfer is measured by local Nusselt number (Nu_x) which can be written as[30]

$$Nu_x = \frac{h_x D_h}{\lambda_f} \qquad (38)$$

The average Nusselt number ($\overline{Nu}$) can be obtained by[30]

$$\overline{Nu} = \frac{1}{L}\int Nu_x \partial x \qquad (39)$$

where $h_x$is the local convective heat transfer coefficient.

The average Nusselt number of a smooth channel (Nu_0) is calculated using the correlation of Dittus and Boelter [32] which shows a consistent agreement with low Reynolds number and is given by

$$Nu_0 = 0{,}023.\mathrm{Re}^{0,8}\,\mathrm{Pr}^{0,4} \quad \text{for} \quad \mathrm{Re} \ge 10^4, \text{heating} \qquad (40)$$

The f_0 and Nu_0 are used as references to minimize the Reynolds number effect in the presented results.

3.3. Grid system

Non-uniform grids with refinements near the all solid boundaries were used in the given computational domain to improve the calculation accuracy of the boundary layer, with the boundary layer effects of fluid flow taken into account [8], as shown in Fig.1(c). To analyze the effect of the grid size on the numerical solution values of f/f_0 and $\overline{Nu}$/Nu_0, various mesh values were verified. Table IIIpresents the percent errors δ and δ' defined as [33]

$$\delta = \left(\frac{\left|\overline{Nu}\right|_{ref} - \overline{Nu}\right|}{\left|\overline{Nu}\right|_{ref}} \right) \times 100 \qquad (41)$$

and

$$\delta' = \left(\frac{\left|f\right|_{ref} - f\right|}{\left|f\right|_{ref}} \right) \times 100 \qquad (42)$$

for meshes of seven sizes in X and Y directions with 220 × 75, 270 × 75, 320 × 95, 370 × 115, 370 × 145, 370 × 160 and 420 × 160 cells. The number within brackets gives the percentage deviation relative to the 420 × 160 cells.

x	y	$\overline{Nu}$/Nu_0	δ (%)	f/f_0	δ' (%)
220	75	10.499	11.435	94.116	-03.835
270	75	11.024	07.003	92.462	-02.011
320	95	11.143	05.999	91.753	-01.229
370	115	11.477	03.187	91.521	-00.973
370	145	11.718	01.155	90.050	00.650
370	160	11.607	02.090	89.731	01.002
420	160	11.855	00.000	90.640	00.000

Table III. Effect of special resolution on the numerical solution at the surface of the upper channel wall for Re = 8.73×10^4

As shown in this table, the mesh with the system of 370 × 145 cells with finer resolution near the walls is selected as the best grid size in the present simulation, which is illustrated in Fig.1(c).

3.4. Numerical model validation

In this section, the verification is conducted to ensure that the analysis is reliable. La verification of the numerical solution the present rectangular channel with two-CRTFs is conducted by comparison with the previous values under similar operating condition as shown in Fig. 2.

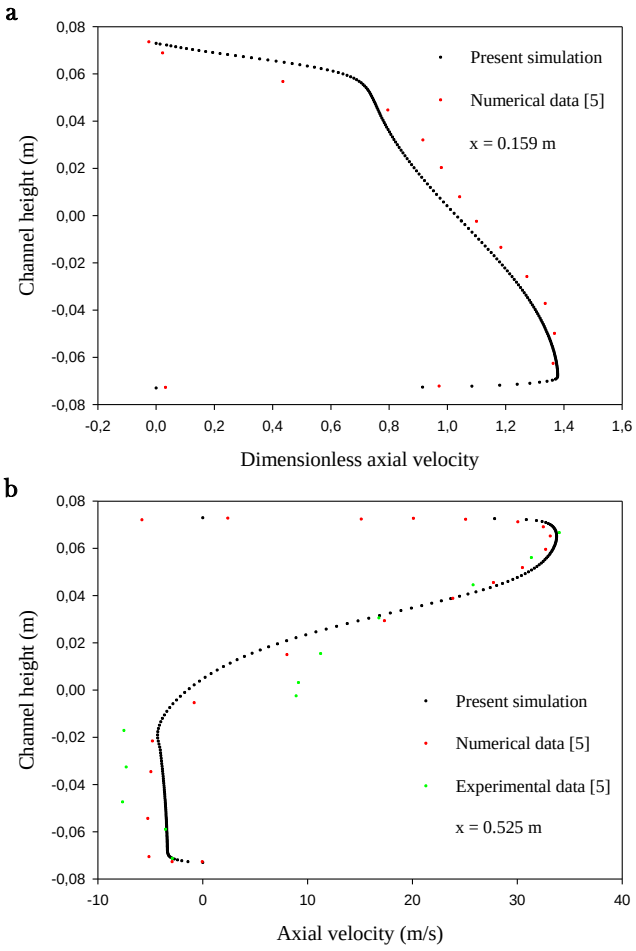

Fig. 2.Validation of the axial velocity distribution with numerical and experimental data [5] at positions (a) x = 0.159 m, and (b) x = 0.525 m, Re = 8.73 × 10⁴

The plots of axial velocity profiles obtained from the current computational analysis are compared with the axial velocity profile plots from the experimental analysis of Demartini et al. [5]. As shown in the figure, our CFD results are in good agreement with the published numerical and experimental data [5]. These comparisons give confidence that the numerical model of the computational analysis used was accurate.

4. Results and discussion

4.1. Fluid flow characteristics

The fluid flow structure in the given computational domain with CRTFs on the opposite channel surfaces can be shown by considering the plots of stream functions as presented in Fig.3(a)-(e). The stream functions in this figure are presented at h = 0.08 m, a/b = 0.25, c = 0.01 m, and Re = 10,000 with five variousCRTF separation distances, i.e., S = Pi/2, 3Pi/4, Pi, 5Pi/4 and 3Pi/2.

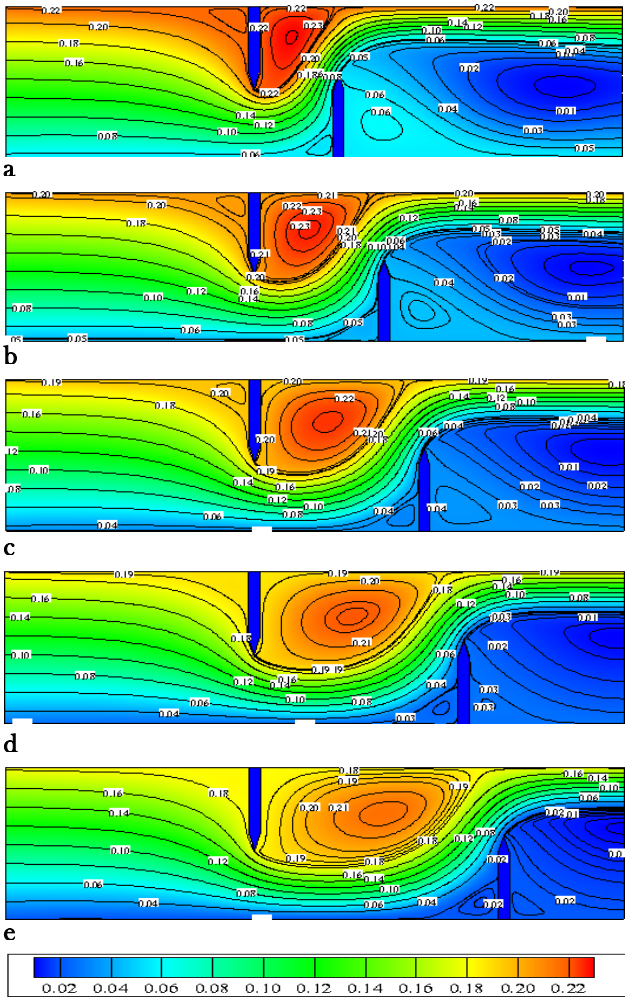

Fig. 3. Variation of streamlines with CRTF spacing for Re = 10,000 and (a) S = Pi/2, (b) S = 3Pi/4, (c) S = Pi, (d) S = 5Pi/4, and (e) S = 3Pi/2

The comparison of streamline plots at different CRTF spacings (Ss) shows that as the fluid flow is accelerated and redirected near the fins, a very small recirculation zone is formed in the vicinity of the upper left corner. In the regions downstream, as a result of sudden expansion in the cross-section, the flow separates, a larger recirculation zone is formed just after the first fin in the upper part of the channel and air flow reattachment is then established. A similar comportment is found near the second fin in the lower part of the channel with recirculation zones at the upstream and downstream CRTF. This observation is confirmed by Mohammadi Pirouz et al. [13]. In addition, higher CRTF separation distance causes the reduction of the velocity of air flow but provides more longitudinal flow leading to the decrease of skin flow resistance [30].

The effects of the CRTF spacing with five values (S = Pi/2, 3Pi/4, Pi, 5Pi/4 and 3Pi/2) for using the 0.25 CRTFs on aerodynamic fields in the given computational whole is also presented in terms of axial velocity fields for the same Reynolds number (Re = 10,000) in Fig. 4(a)-(e), respectively.

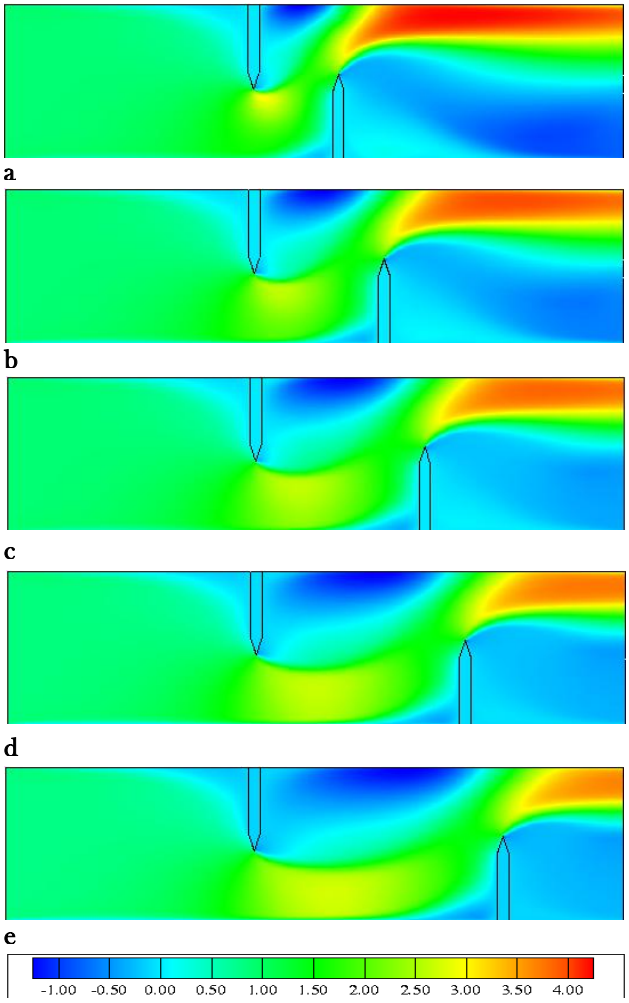

Fig. 4. Variation of axial velocity fields with CRTF spacing for Re=10,000 and (a) S = Pi/2, (b) S = 3Pi/4, (c) S = Pi, (d) S = 5Pi/4, and (e) S = 3Pi/2

The maximum axial velocity values are seen near the upper channel wall with an acceleration process that starts just after the second CRTF, while the axial velocity field is observed to be very low adjacent to the CRTFs, in accordance with the results by Demartini et al. [5]. A large recirculation cell with very low velocity values (negative velocities) is found between the CRTFs close to the main flow with yields the strong influence of air velocity on heat transfer enhancement, as confirmed numerically by Nasiruddin and Kamran Siddiqui [8], and Sripattanapipat and Promvonge [30].Reducing the separation distance (S) in the axial direction makes the flow deviate and accelerate in the vicinity of fin faces, and causes an increase in the deformation of the flow field, and thus the disruption of the fluid flow is inversely proportional to the distance between CRTFs, as indicated and confirmed by Mohammadi Pirouz et al. [13].

The contour plots of the dynamic pressure coefficient are shown in Fig. 5 for different CRTF distances (S).

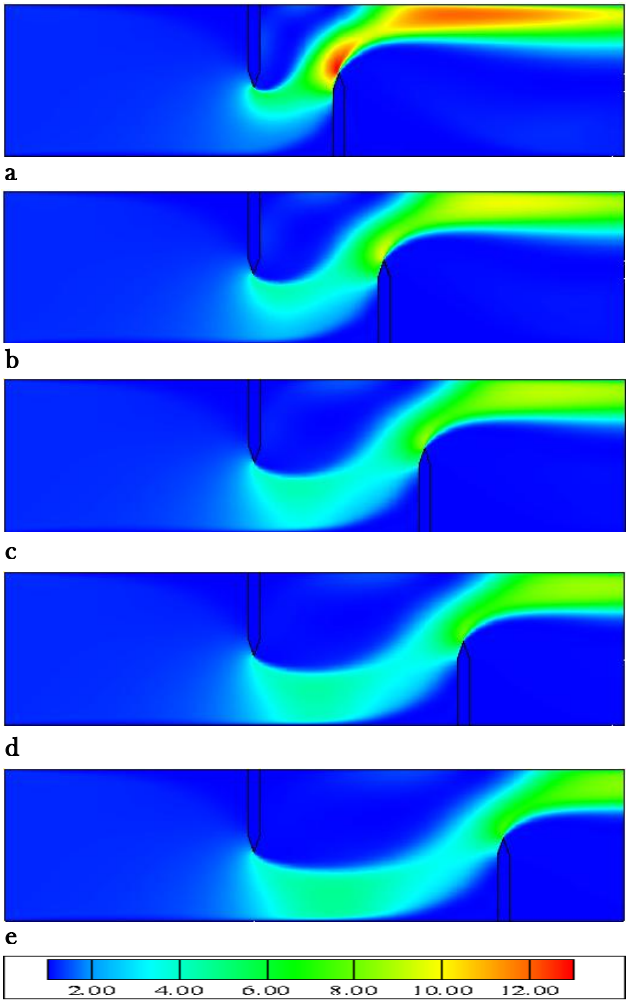

Fig. 5. Variation of dynamic pressure fields with CRTF spacing for Re = 10,000 and (a) S = Pi/2, (b) S = 3Pi/4, (c) S = Pi, (d) S = 5Pi/4, and (e) S = 3Pi/2

Similar to the results in Fig. 4, the largest variations are found near the CRTF tips, due to the strange velocity gradients in those regions [5].

Fig. 6 presents the dimensionless axial velocity profiles (U/U_{in}) at various axial locations (x = 0.159, 0.189, 0.255, 0.285, 0.315, 0.345 and 0.525 m) in the channel for using the 0.25 CRTFs with h = 0.08m, c = 0.01 m and S = Pi. In the figure, the U/U_{in} values are related as a function of Reynolds number.

Fig. 6(a) displays the axial U/Uin profile along the height of the channel with both positions x = 0.159 m and x = 0.189 m, measured downstream of the entrance, respectively 0.059 m and 0.029 m before the first CRTF. It is seen in the figure that the effect of the perturbation of the airflow field increases as the flow approaches the upper

wall-attached CRTF, increasing the velocity of the fluid flow approaching the passage under the considered fin [5].

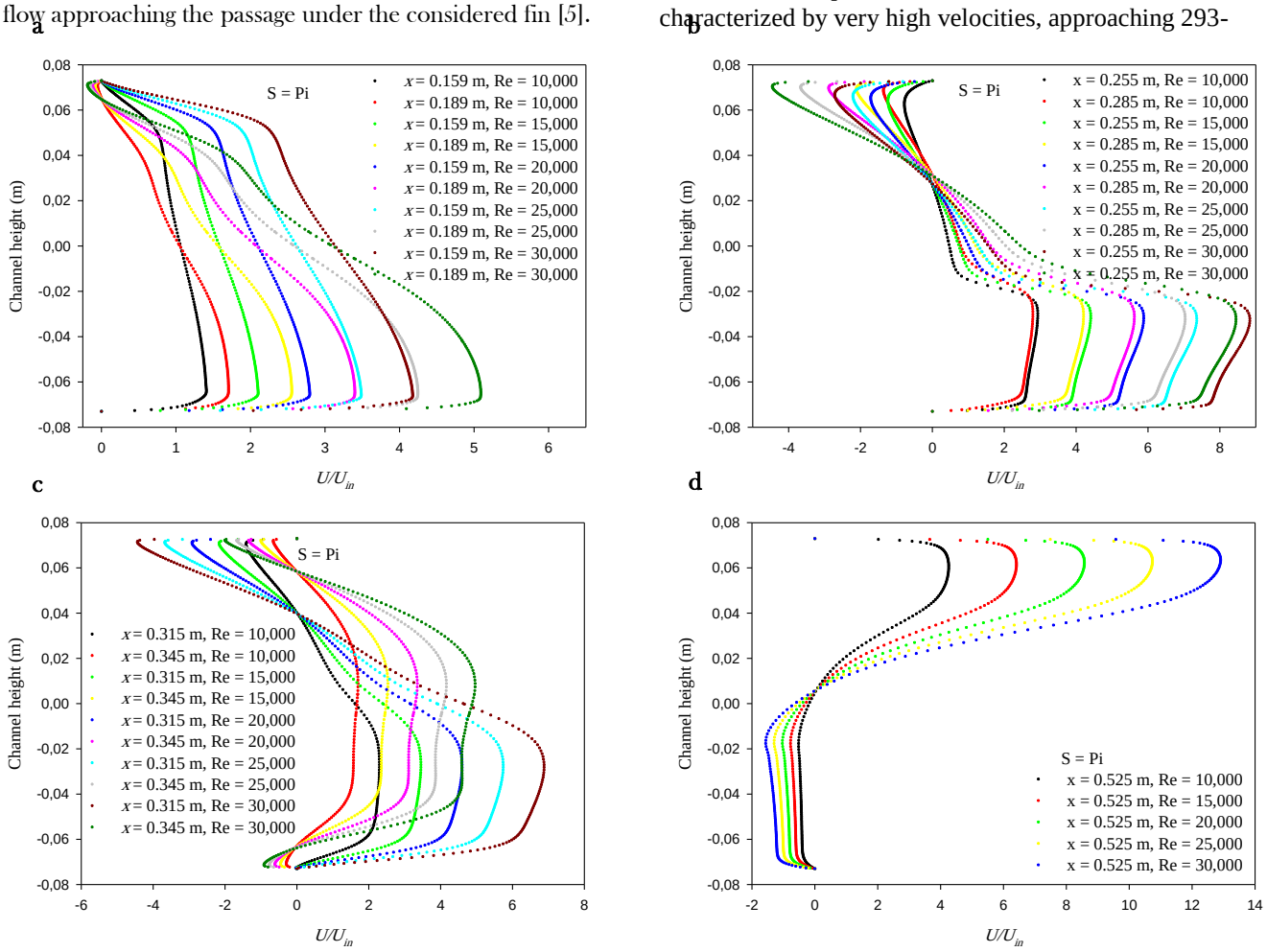

Fig. 6.Distribution of dimensionless axial velocity profiles as a function of Reynolds number in various transverse sections for S = Pi and (a) Upstream of the upper wall CRTF at x = 0.159 m and x = 0.189 m, (b) between both CRTFs at x = 0.255 m and x = 0.285 m, (c) upstream of the lower wall CRTF at x = 0.315 m and x = 0.345 m, and (e) behind the lower wall CRTF, near the channel outlet at x = 0.525 m

Fig. 6(b) shows the dimensionless axial velocity profiles downstream of the first CRTF at positions given by x = 0.255 m and x = 0.285 m from the entrance, while Fig. 6(c) shows the results of U/Uin upstream of the second CRTF at locations x = 0.315 m and x = 0.345 m from the channel inlet, respectively 0.055 m and 0.025 m before the lower wall fin. In the upper part of the channel, a strong recirculation zone with very low velocity values is observed behind the first CRTF, which was induced due to the flow separation [8]. The recirculation cell was located close to the solid wall [8] and its height was approximately equal to the extent of the flow blockage by the CRTF, which is equal to 0.08 m for the cases shown in Fig. 6.

The reverse flow downstream of the upper wall CRTF causes the fluid to strongly rotating motion. This motion causes the air near the wall to flow in the core region and vice versa [30]. The size of this recirculation zone is found to be larger than the ones at the corner[30] (a small one at the top left corner upstream of the first fin and a small one at the bottom left corner before the second fin). In the lower part of the channel, the airflow is characterized by very high velocities, approaching 293-883% of the reference velocity, depending on the Reynolds number values (see Fig. 6(b)).

Between the CRTFs, the U/U_{in} profiles show that as the airflow approaches the lower wall CRTF, its velocity is reduced in the lower part of the channel, while in the upper part is increased [5], as shown in Fig. 6(c).

Downstream of the second CRTF, at x = 0.525 m, 0.029 m before channel outlet, the highest velocity values are found near the upper channel wall with an acceleration process that starts just after the lower wall CRTF, as shown in Demartini et al. [5]. This fact is associated to the negative velocities at the channel outlet [5] shown in Fig. 6(d). Concerning the effect of the Reynolds number on the fluid velocity, it can see from this figure and for this CRTF spacing (S = Pi), that the U/U_{in} value tends to increase with the rise of Reynolds number values for all axial locations examined. By augmenting the Re from 10,000 to 30,000, the flow of air reattaches on the CRTF wall and back areas, while reverse flow lengths are increased.

The lengths of recirculation zones are also affected by the CRTF spacing value (S). Fig. 7 depicts the dimensionless axial velocity profiles a function of the distance of separation between the CRTFs. In this case, the Reynolds number is kept constant at a value of 10^4. It is shown that the larger recirculation zone can be found in the region downstream for S = Pi/2. The smaller the CRTF spacing, the longer the recirculation zone becomes.

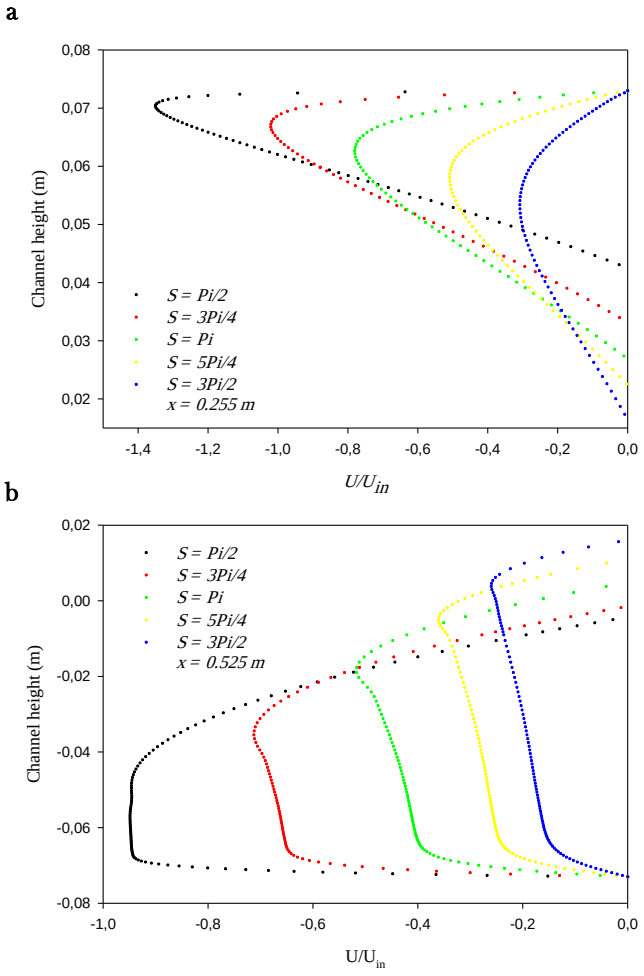

Fig. 7. Effect of S on U/U_{in} in the regions downstream of both CRTFs for Re = 10^4at(a) x = 0.255 m, and(b) x = 0.525 m

4.2. Heat Transfer

The computational results on convective heat transfer aspects in a constant temperature-surfaced rectangular channel mounted with two 0.25 CRTFs of various horizontal distances between the CRTFs are presented in the form of Nusselt numbers, which are calculated from their definition as given in Eqs. (38) and (39).

Fig. 8(a)-(c) shows the local Nusselt number, Nu_x along the heated top surface, Y = H/2 of the channel for different CRTF spacing values (S = Pi/2, 3Pi/4, Pi, 5Pi/4 and 3Pi/2) in the cases of different Reynolds number values (Re = 10,000, 20,000 and 30,000), respectively. In the given configuration, the first cascaded rectangular-triangular fin (CRTF) with a/b = 0.25 is attached to the heated top surface while the second CRTF is attached to the heated bottom surface. The local Nusselt number is high at the start of the heating section due to the development of the thermal boundary layer, as indicated by Dutta and Hossain [15].The placement of the first fin at the beginning of the heated section (L_1 = 0.218 m)

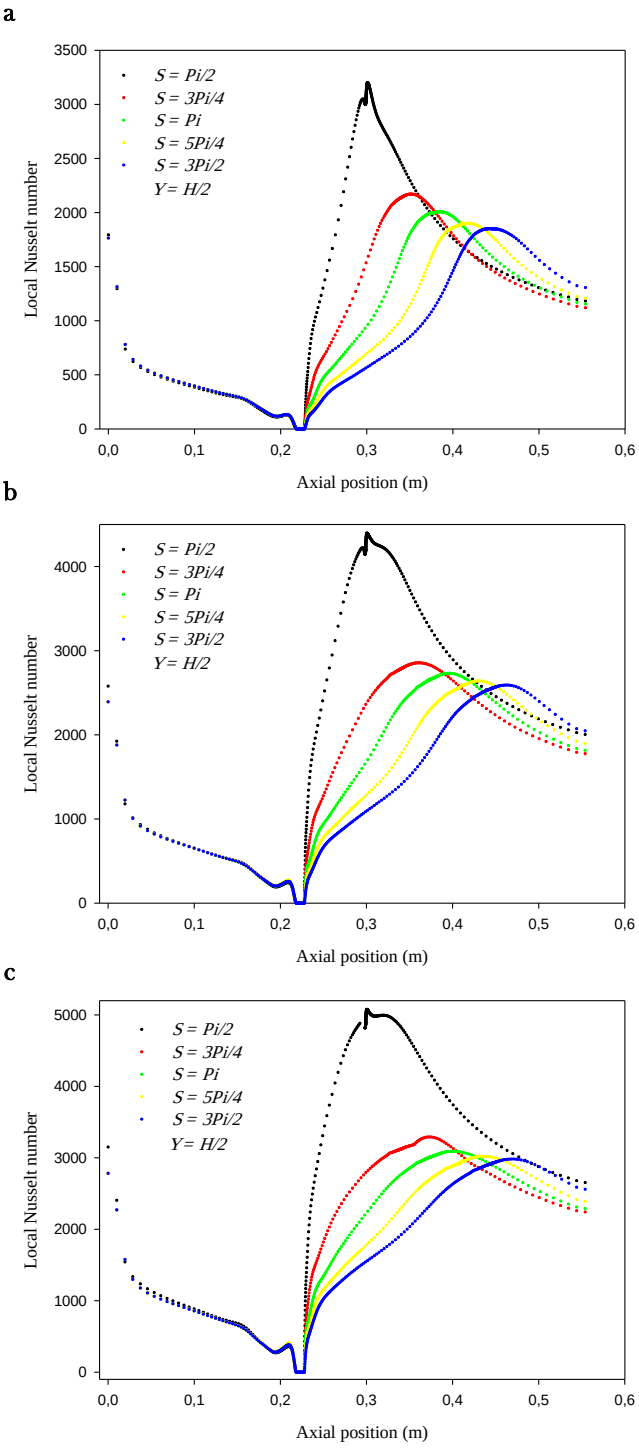

Fig. 8. Variations of local Nusselt number as a function of CRTF spacing along the upper channel wall for various

Reynolds number values (a) Re = 10,000, (b) Re = 20,000, and (c) Re = 30,000

disturbs the boundary layer formation and contributes to higher heat transfer [15]. It is found that the Nu_x varies from 1750 to 3150 at the thermal entry region, depending on the Reynolds number values. At $0 \le x \le 0.218$ m, the Nu_x value shows a decrease and then down when approaching the upper wall CRTF (for $0.218 \le x \le 0.228$ m) for all fin spacing values examined. In the region downstream of the first CRTF at the locations corresponding to the zone of recirculation as seen in the figure, the Nu_x profiles show an increase gradually until reaching the second CRTF area where maximum Nu_x value occurs and then shows an abrupt reduction through the exit. These results are confirmed numerically by Sripattanapipat and Promvonge [30].For using the CRTFs, it is observed from the figure that the decrease in the separation distance between the considered fins (S) from 3Pi/2 to Pi/2 leads to a higher Nusselt number. The variation of Nu_x with Reynolds number for all cases is also depicted in Fig. 8(a)-(c). It is clear from this figure that the Nu_x increases with the increase of Reynolds number, as expected.

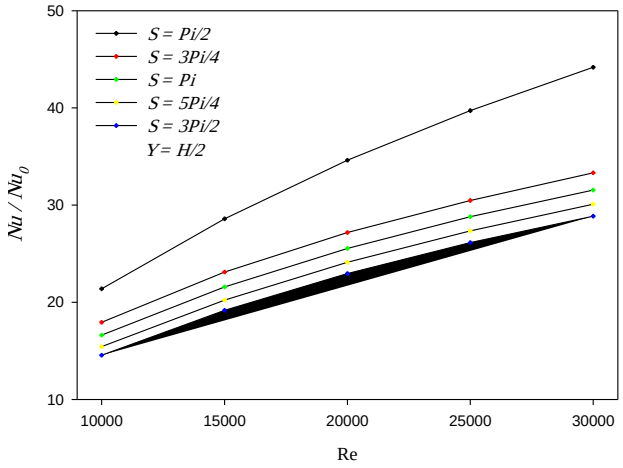

Fig. 9.Variations of Nu/Nu_0 with Reynolds number for various distances between CRTFs

The effects of the spacing value with five horizontal distance between the fins (S = Pi/2, 3Pi/4, Pi, 5Pi/4 and 3Pi/2) for using the 0.25 CRTFs on average heat transfer rate in the form of Nu/Nu_0 are presented in Fig. 9. In the figure, the Nu/Nu_0 is related as a function of Reynolds number $10,000 \le Re \le 30,000$. The result obtained from the plain channel with no fins is also presented for comparison. In the figure, it is interesting to note that the Nu/Nu_0 value tends to increase with the rise of Reynolds number values for all CRTF spacing values. It is also noted that the Nu/Nu_0 increases with decreasing the S, apart from Re values and thus, the S = Pi/2 provides maximum heat transfer rate. This is because the shorter fin spacing interrupts the development of the boundary layer of the fluid flow and increases the turbulence intensity of the flow [34]. In addition, the CRTF with S = Pi/2 at $10,000 \le Re \le$

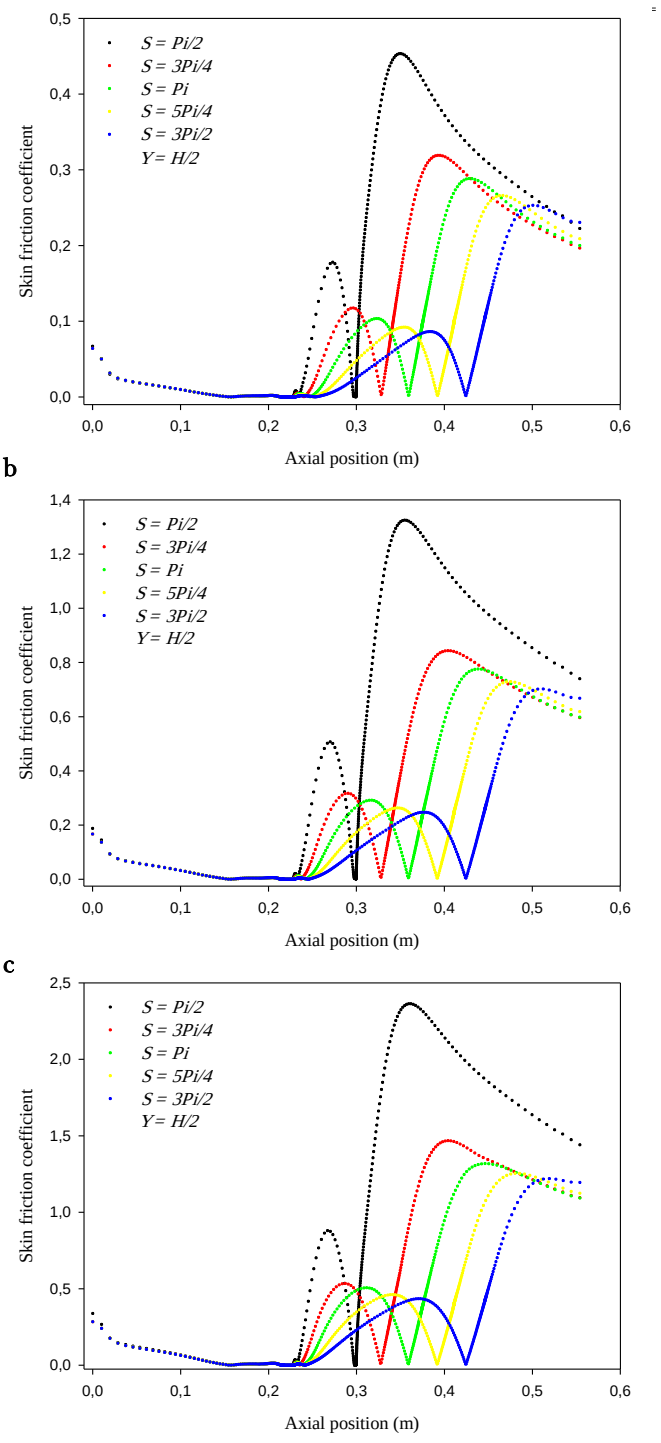

Fig. 10.Variations of skin friction coefficient as a function of CRTF spacing along the upper channel wall for various Reynolds number values (a) Re = 10,000, (b) Re = 20,000, and (c) Re = 30,000

Pi, S = 5Pi/4, and S = 3Pi/2 around 16.11-24.58%, 22.27-24.58%, 27.82-31.89% and 31.93-34.68%, respectively.

Also, the channel fitted with CRTFs gives higher values of Nu/Nu_0 than that for smooth rectangular air channel with no fins due to 'the induction of high recirculation zones and thin boundary layer' in the finned channel, leading to 'higher temperature gradients' [34] for all cases investigated.

4.3. Friction loss

Fig.10 shows the variation of the skin friction coefficient, Cf with different spacing values of the CRT fins at a/b = 0.25 and various Re values. In the figure, the skin friction is observed to be very low in the region upstream of the upper wall CRTF for all cases investigated. The latter is produced by the orientation of airflow by the first CRTF towards the lower part of the channel. The skin friction coefficient is increased at the locations corresponding to the cells of recirculation downstream of the upper wall CRTF as seen in the figure. Due to the changes in the airflow direction produced by the CRTFs, the highest skin friction values appear near the tip of the lower wall CRTF due to the strong velocity gradients in that region with an acceleration process that starts just after the second CRTF [5]. In addition, substantial increases in Cf values are found for the rise in Reynolds number and/or for the decrease in CRTFseparation values.

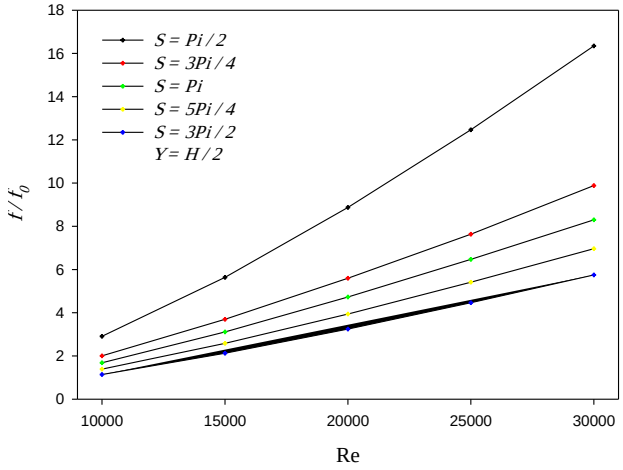

Fig. 11.Variations of f/f_0 with Reynolds number for various distances between CRTFs

Fig.11 shows the variation of friction factor rate, f/f_0 with the CRTF spacing (S = Pi/2, 3Pi/4, Pi, 5Pi/4 and 3Pi/2) for different values of flow Reynolds number ($10{,}000 \leq Re \leq 30{,}000$). We note that the f/f_0 tends to increase with the rise of Re for all CRTF spacing cases. The cascaded rectangular-triangular finned channel is seen to yield higher f/f_0 than the plain channel with no fins channel. The f/f_0 values for the channel with two-CRTFs appear to be about 1.14-16.34 times above those for the channel with no fins, depending on the S and Re values. What was also noticed, the f/f_0 for air flowing in the finned channel with smaller CRTF spacing (S) is found to be higher than that with larger S. The f/f_0 increases with the decrease of CRTF spacing and thus, the Pi/2 provides maximum friction factor ratio, in which there is more flow resistance.

5. Conclusion

Through this work, we performed a two-dimensional analysis of a constant property fluid (air) flowing into a rectangular cross section channel with staggered cascaded rectangular-triangular shaped fins (CRTFs). The governing flow equations, i.e., continuity, momentum, turbulence, and energy equations, employed to simulate the incompressible steady fluid and heat transfer in the whole domain investigated, were solved by the finite volumes approach, in two dimensions, employing the Computational Fluid Dynamics, Commercial Software FLUENT with the low-Reynolds-number k-ε model to describe the turbulence phenomenon. The effects of Reynolds number as well as CRTF separation distance on the thermo-aeraulic fields were investigated. Substantial increases in Nusselt number and friction factor values are found for the rise in Reynolds number and/or for the decrease in CRTF spacing values.This analysis can be applied in improving the thermal efficiency of solar air collectors as well as heat exchangers.

Nomenclature

a	triangular fin height, m
b	cascaded fin height, m
c	base thickness, m
Cf	skin friction coefficient
Cp	specific heat at constant pressure J kg^{-1} K^{-1}
$C_{1\varepsilon}$	constant used in the standard k-ε model
$C_{2\varepsilon}$	constant used in the standard k-ε model
C_{μ}	constant used in the standard k-ε model
D_h	hydraulic diameter of the rectangular channel, m
f	friction factor
G	production rate of the kinetic energy, $m^2 s^{-2}$
H	Height of air tunnel in channel, m
h_x	local convective heat transfer coefficient, W $m^{-2}K^{-1}$
k	turbulent kinetic energy, $m^2 s^{-2}$
L	channel length, m
L_1	distance upstream of the first cascaded fin, m
L_2	distance downstream of the second cascaded fin, m
$\overrightarrow{N}$	coordinate normal to the wall
Nu_x	local Nusselt number
$\overline{Nu}$	average Nusselt number
P	fluid pressure, Pa
P_{atm}	atmosphericpressure, Pa
Pi	cascaded fin distance or spacing, m
Pr	Prandtl number
Re	Reynolds number
T	temperature, K
T_{in}	inlet temperature, K
T_w	wall temperature, K
U_{in}	inlet velocity, m/s

$\overline{U}$ channel average velocity, m s^{-1}
u fluid velocity in the x-direction, m s^{-1}
v fluid velocity in the y-direction, m s^{-1}
x, y Cartesian coordinates, m

Greek symbols

ε turbulent dissipation rate, m^2 s^{-3}
Γ_ϕ coefficient of turbulent diffusion
λ_f thermal conductivity of fluid, W m^{-1} °C^{-1}
λ_s thermal conductivity of solid, W m^{-1} °C^{-1}
μ dynamic viscosity, Kg m^{-1} s^{-1}
μ_e effective viscosity, Kg m^{-1} s^{-1}
μ_l laminar viscosity, Kg m^{-1} s^{-1}
μ_t eddy viscosity, Kg m^{-1} s^{-1}
ν kinematics viscosity, Kg m^{-1} s^{-1}
ρ fluid density, kg m^{-3}
σ_k constant used in the standard k-ε model
σ_ε constant used in the standard k-ε model
σ_T constant used in the standard k-ε model
τ_w wall shear stress, Pa
ψ stream function, Kg s^{-1}
ϕ stands for the dependent variables u, v, T, k and ε
ΔP pressure drop, Pa
S_ϕ limit of source for the general variable ϕ

Subscript

atm atmospheric
e effective
f fluid
in inlet of the channel
l laminar
s solid
t turbulent
w wall

References

[1] C. Berner, F. Durst, D.M. McEligot, *Trans. ASME J. Heat Transfer* 106 (1984) 743-749
[2] K.M. Kelkar, S.V. Patankar, *ASME J. Heat Transfer* 109 (1987) 25-30
[3] J.R. Lopez, N.K. Anand, L.S. Fletcher, *Numer. Heat Transfer*, A Appl. 30 (1996) 189-205
[4] Y.L. Tsay, J.C. Cheng, T.S. Chang, *Numer. Heat Transfer*, A Appl. 43 (8) (2003) 827-841
[5] L.C. Demartini, H.A. Vielmo, S.V. Möller, *J. of the Braz. Soc. of Mech. Sci. & Eng.* 26(2) (2004) 153-159
[6] M.A. Habib, A.M. Mobarak, M.A. Sallak, E.A. Abdel Hadi, R.I. Affify, Trans. *ASME J. Heat Transfer* 116 (1994) 363-368
[7] S.S. Mousavi, K. Hooman, *Energy Convers. Manag.* 47 (2006) 2011-2019
[8] Nasiruddin, M.H. Kamran Siddiqui, *Int. J. Heat and Fluid Flow*, 28(2) (2007) 318-328
[9] B.H.L. Gowda, B.A.A. Achar, M. Hasan, K. Prasanna Kumar, M. Shuja, T.L.S. Rao, Dipak Sen, Proc. 37th National & 4th Int. Conf. on Fluid Mechanics and Fluid Power, IIT Madras, Chennai, India,16-18 Dec. 2010
[10] M. Saffar-Avval, E. Damangir, *Int. J. Heat Mass Transfer* 38 (1995) 2501-2506
[11] H. Li, V. Kottke, *Int. J. Heat Mass Transfer* 41(10) (1998) 1303-1311
[12] Y.L. Tsay, T.S. Chang, *J.C. Cheng, Acta Mech.* 174 (2005) 63-76
[13] M. Mohammadi Pirouz, M. Farhadi, K. Sedighi, H. Nemati, E. Fattahi, *Scientia Iranica B* 18(2) (2011) 213-221
[14] P. Dutta, S. Dutta, *Int. J. Heat Mass Transfer* 41 (1998) 3005-3013
[15] P. Dutta, A. Hossain, *Int. J. Heat and Fluid Flow*, 26 (2005) 223-232
[16] S. Dutta, P. Dutta, R.E. Jones, J.A. Khan, *ASME J. Heat Transfer* 120 (1998) 795-797
[17] Y. Menni, A. Azzi, C. Zidani,*Communication Science & technology* 17 (2016) 67-77
[18] Y. Menni, A. Azzi, C. Zidani, *Revue des Energies Renouvelables* 18(3) (2015) 347-361
[19] Y. Menni, C. Zidani, A. Azzi, B. Benyoucef, *Revue des Energies Renouvelables* 19(2) (2016) 235-250
[20] Y. Menni, A. Azzi, C. Zidani, *Communication Science & technology*16 (2016) 34-43
[21] Y. Menni, A. Azzi, C. Zidani, *Communication Science & technology*18 (2017) 43-57
[22] Y. Menni, A. Azzi, C. Zidani, *Journal of Engineering Science and Technology* 12(12) (2017) 3251-3273
[23] Y. Menni, A. Azzi , C. Zidani, B. Benyoucef, *Journal of New Technology and Materials* 06 (2) (2016) 44-55
[24] Y. Menni, A. Azzi , C. Zidani, *Courrier du Savoir*23 (2017) 75-84
[25] Y. Menni, A. Azzi, C. Zidani, *Revue des Energies Renouvelables* 19 (3) (2016) 345-366
[26] W. P. Jones, B. E. Launder, *Int. J. Heat Mass Transfer* 16(6) (1981) 1119-1130
[27] S.V. Patankar, Numerical heat Transfer and fluid flow, McGraw-Hill, New York, 1980
[28] B.E. Launder, D.B. Spalding, *Computer Methods in Applied Mechanics and Engineering,* 3 (1974) 269-289
[29] J.P. Van Doormaal, G.D. Raithby, *Numerical HeatTransfer* 7 (1985) 147-163
[30] S. Sripattanapipat, P. Promvonge, *Int. Commun. Heat Mass Transfer* 36(1) (2009) 32-38
[31] B.S. Petukhov, Heat transfer in turbulent pipe flow with variable physical properties. In: Harnett JP, editor. *Advances in heat transfer*, New York: Academic Presss, 6(1970) 504-564
[32] F.W. Dittus, L.M.K. Boelter, Heat transfer in automobile radiators of tubular type, Univ. California, Berkeley, Publ. Engineering, 1(13) (1930) 755-758
[33] Nicolau B. Santos, Marcelo J. S. de Lemos, *Numerical Heat Transfer*, Part A, 49 (2006) 471-494
[34] P. Sriromreun, C. Thianpong, P. Promvonge, *Int. Commun. Heat Mass Transfer* 39 (2012) 945-952